

Regulation of AMPA receptor channels and synaptic plasticity by cofilin phosphatase Slingshot in cortical neurons

Eunice Y. Yuen¹, Wenhua Liu¹, Tal Kafri³, Henriette van Praag² and Zhen Yan¹

¹Department of Physiology and Biophysics and New York State Center of Excellence in Bioinformatics and Life Sciences, State University of New York, Buffalo, NY 14214, USA

²Neuroplasticity and Behavior Unit, Laboratory of Neurosciences, National Institute of Aging, Baltimore, MD 21224, USA

³Gene Therapy Center, University of North Carolina at Chapel Hill, 7119 Thurston Bowles, CB 7352, Chapel Hill, NC 27599, USA

Cofilin, the major actin depolymerizing factor, modulates actin dynamics that contribute to spine morphology, synaptic transmission and plasticity. Much evidence implicates the cofilin inactivation kinase LIMK in synaptic function, but little is known about the cofilin activation phosphatase Slingshot in this regard. In this study, we found that suppressing endogenous Slingshot with small RNA interference or function-blocking antibody led to a dramatic reduction of AMPA receptor-mediated excitatory postsynaptic currents (EPSCs) in cortical neurons. Perturbation of Slingshot function also diminished the ability to express synaptic plasticity. Inactivating cofilin or disturbing actin dynamics reduced AMPAR-EPSCs in a Slingshot-dependent manner. Moreover, surface GluR 1 and synaptic GluR2/3 clusters were reduced by Slingshot knockdown. Our data suggest that Slingshot plays a pivotal role in AMPAR trafficking and synaptic transmission by controlling actin cytoskeleton via cofilin activation.

(Received 18 December 2009; accepted after revision 30 April 2010; first published online 4 May 2010)

Corresponding author Z. Yan: Department of Physiology and Biophysics, State University of New York at Buffalo, 124 Sherman Hall, Buffalo, NY 14214, USA. Email: zhenyan@buffalo.edu

Abbreviations CaMKII, Ca²⁺-calmodulin-dependent protein kinase II; GFP, green fluorescent protein; GluR, ionotropic glutamate receptor; LIM kinase, cofilin inactivation kinase; LTP, long-term potentiation; mEPSC, miniature excitatory postsynaptic current; shRNA, short hairpin RNA; siRNA, small interfering RNA; SSH, Slingshot.

Introduction

Actin cytoskeleton, which is enriched at the synapses, plays a pivotal role in spine morphology (Okamoto *et al.* 2004), receptor anchoring/trafficking and synaptic plasticity (Fukazawa *et al.* 2003). Several mechanisms have been suggested for actin dynamics to regulate the AMPA receptor (AMPA) channel, an ionotropic glutamate receptor (GluR) that governs most of the excitatory synaptic transmission in central neurons (Derkach *et al.* 2007). Actin anchors existing AMPARs at the synaptic membrane through direct binding of the actin linker 4.1N to GluR1 (Shen *et al.* 2000) or the PDZ domain protein PICK1 to GluR2 (Rocca *et al.* 2008), and disruption of these linkages promotes AMPAR internalization (Shen *et al.* 2000; Rocca *et al.* 2008). In addition, myosin, the motor protein that moves on actin cytoskeleton, contributes to the trafficking of AMPARs to dendrites and spines (Lise *et al.* 2006; Correia *et al.* 2008; Wang *et al.* 2008). Perturbing actin assembly impairs

AMPA-mediated synaptic plasticity (Fukazawa *et al.* 2003), while on the other hand, actin polymerization and depolymerization are strongly modulated by synaptic plasticity (Okamoto *et al.* 2004; Lin *et al.* 2005). These lines of evidence suggest that AMPAR function can be profoundly affected by actin dynamics.

The dynamics of actin assembly is regulated by several important factors, one of which is the cofilin protein, a major actin depolymerizing factor controlling the equilibrium between filamentous and monomeric actin (dos Remedios *et al.* 2003; Huang *et al.* 2006). Cofilin is inactivated by LIM kinase (LIMK)-mediated phosphorylation at Ser3, and is reactivated by Slingshot-mediated dephosphorylation (Agnew *et al.* 1995; Huang *et al.* 2006). The dephosphorylated cofilin binds to F-actin, leading to actin severing and depolymerization. Studies in *Drosophila* show that knockdown of Slingshot profoundly impairs actin reorganization and cellular architecture (Niwa *et al.* 2002), suggesting the crucial role of Slingshot in

actin-based processes. While many studies have linked LIMK to mental retardation, impaired synaptic plasticity and abnormal spine morphology (Meng *et al.* 2002), little is known regarding the physiological function of Slingshot in neurons. Here, we investigated the role of Slingshot in regulating AMPAR trafficking and synaptic transmission in cortical neurons, and the involvement of cofilin-regulated actin dynamics.

Methods

Electrophysiological recordings

All experiments were performed with the approval of the Institutional Animal Care and Use Committee (IACUC) of the State University of New York at Buffalo, and our animal care procedures were in accordance with the IACUC guidelines under the Animal Welfare Act. In brief, rats were anaesthetized with halothane vapour before decapitation. Cortical cultures from embryonic day (E)18 rats or cortical slices from postnatal rats (3–4 weeks) were prepared as described previously (Yuen *et al.* 2005; Yuen & Yan, 2009). The whole-cell voltage-clamp technique (Gu *et al.* 2006; Yuen & Yan, 2009) was used to measure mEPSCs in cultured neurons (DIV 21–24). The external solution contained (mM): 127 NaCl, 5 KCl, 2 MgCl₂, 2 CaCl₂, 12 glucose, 10 Hepes, 0.001 TTX, pH 7.3–7.4, 300–305 mosmol l⁻¹. 2-amino-5-phosphonovaleric acid (APV; 25 μM) and bicuculline (10 μM) were added to block NMDARs and GABA_ARs. The internal solution contained (in mM): 130 caesium methanesulfonate, 10 CsCl, 4 NaCl, 1 MgCl₂, 10 Hepes, 5 EGTA, 2.2 QX-314, 12 phosphocreatine, 5 MgATP, 0.5 Na₂GTP, pH 7.2–7.3, 265–270 mosmol l⁻¹. The membrane potential was held at -70 mV. Recordings were performed using an Axopatch 200B amplifier. Tight seals were generated by applying negative pressure, followed by additional suction to disrupt the membrane and obtain the whole-cell configuration. To record mEPSCs in slices, a modified ACSF containing a low concentration of MgCl₂ (1 mM) and TTX (1 μM) was used.

To measure evoked AMPAR-EPSCs (Yuen *et al.* 2007), cortical slices (300 μm) were bathed in ACSF containing APV (25 μM) and bicuculline (10 μM). The internal solution was the same as that used for mEPSC recording of cultured neurons. Evoked NMDAR-EPSC was recorded as previously described (Yuen *et al.* 2005). Recordings were performed using a Multiclamp 700A amplifier. Neurons were visualized with a ×40 water-immersion lens and illuminated with near infrared light. Cells were clamped at -70 mV. EPSCs were stimulated by exciting the neighbouring cortical neurons with a bipolar tungsten electrode (FHC, Inc.) located at a few hundred micrometres away from the neuron being recorded. To

generate the input–output responses, a series of different stimulation intensities (5–9 V) with the same duration of pulses (0.05 ms) was used to elicit synaptic currents. To minimize experimental variations between cells, the following criteria were used: (1) the stimulating electrode was positioned at the same location from the cell being recorded; (2) layer V prefrontal cortical pyramidal neurons with comparable membrane capacitances were selected; (3) recordings from infected and nearby non-infected cells were interleaved throughout the course of experiments.

Miniature synaptic currents were analysed with Mini Analysis Program (Synsoft, Leonia, NJ, USA). Statistical comparisons were made using the Kolmogorov–Smirnov test. Evoked synaptic currents were analysed with Clampfit (Axon Instruments). For analysis of statistical significance, ANOVA tests were performed to compare groups subjected to different drug application or transfection.

Small interfering (si)RNA and lenti-virus short hairpin (sh)RNA

The siRNA-targeting Slingshot was transfected into primary cultures (21 DIV) using Lipofectamine 2000 (Yuen & Yan, 2009). Electrophysiological and immunocytochemical experiments were performed 2–3 days after transfection. Procedures for preparing organotypic cortical slice cultures were as described previously (Stoppini *et al.* 1991). Briefly, frontal brain slices (300 μm) from rat (postnatal day 5) were cut by Vibratome, and then transferred to MilliCell inserts (Millipore) in the presence of Neurobasal medium with N1 medium supplement (Sigma) and 20% horse serum. Media were changed every 2 days. At DIV 7, slices were infected with lenti-virus containing green fluorescent protein (GFP)-tagged Slingshot shRNA (2 μl virus in 1 ml medium). Recordings were performed 1 week post-infection. The lenti-viral vector pTK1168 is an HIV-1-based vector containing the U6-shRNA for Slingshot upstream to an expression cassette comprising the CMV promoter and a sequence encoding the GFP-blasticidin fusion protein. Lenti-virus was prepared by a four-plasmid transient transfection. Specifically, using Lipofectamine 2000 (Invitrogen), 90% confluent human embryonic kidney 293T cells in 10 cm plates were transfected with 22.5 mg pTK1168, 15 mg MDL, 5.7 mg RSV REV and 7.5 mg CMV-VSVG. Seventy-two hours after transfection, supernatant was collected, sterile-filtered, concentrated by 2 × 2 h of ultracentrifugation at 60,000 g. (Sorvall Discovery) and resuspended in 100 μl Dulbecco's PBS (Invitrogen). Both siRNA and shRNA for silencing Slingshot (SSH1L) were generated using the sequence:

5'-UCGUCACCCAAGAAAGUA-3' (Niwa *et al.* 2002; Wang *et al.* 2005). The knockdown efficacy of Slingshot with the SSH1L siRNA was previously demonstrated by immunocytochemical studies (Yuen & Yan, 2009), and also verified here by Western blot analysis with anti-Slingshot1 (1:500, ECM Bioscience).

Immunocytochemistry

To label surface GluR1 subunits, primary cultures (DIV 21–30) were fixed (4% paraformaldehyde, 30 min) without permeabilization, and then blocked (5% BSA, 1 h) to remove non-specific staining. Cells were incubated with anti-GluR1 (N-terminal, 1:500, Millipore, 07-660) at 4°C overnight. After three washes in PBS, cells were incubated with an Alexa 594-conjugated secondary antibody (1:200, Molecular Probes) at room temperature (RT) for 1 h. To label synaptic GluR2 subunits, cultures were fixed, permeabilized, blocked, and incubated with anti-GluR2/3 (1:500; Millipore, AB1506) and anti-synaptophysin (1:500; Sigma, S5768) at 4°C overnight. To visualize F-actin, dendrites were first labelled with anti-MAP2 (Microtubule Associate Protein 2) (1:500; Santa Cruz, sc-20172) at RT for 2 h and an Alexa 488-conjugated secondary antibody at RT for 1 h (1:200, Molecular Probes). Then neurons were incubated with rhodamine phalloidin (1:2000, Molecular Probes, R-415) at RT for 20 min. After washing, coverslips were mounted on slides with Vectashield mounting media (Vector Laboratories).

Fluorescence images were detected using a $\times 100$ objective with a CCD camera mounted on a Nikon microscope. All specimens were imaged under identical conditions and analysed with identical parameters using ImageJ software. Several (3–4) dendritic segments (50 μm) with an equal distance away from the soma were selected on each neuron. For each coverslip, four to six individual neurons were chosen. Clusters were detected with a threshold corresponding to a 2- to 3-fold intensity of the diffuse fluorescence on the dendritic shaft. Three to four independent experiments were performed. Quantitative analyses were performed blindly without knowing the experimental conditions.

Results

Inhibition of Slingshot suppresses AMPA receptor function

To study the physiological role of Slingshot (SSH) in synaptic functions, we suppressed the expression of endogenous SSH with small interference RNA, and then examined the alteration of AMPA receptor-mediated currents in cortical pyramidal neurons. First, we examined miniature EPSCs (mEPSCs), the postsynaptic response

to release of individual vesicles of glutamate, in cultured cortical neurons. The SSH siRNA induced an effective and specific knockdown of SSH expression (Fig. 1A inset, also see Yuen & Yan, 2009). The amplitude and frequency of mEPSCs were significantly smaller in SSH siRNA-transfected neurons (Fig. 1A–C, 12.8 ± 0.9 pA, 2.7 ± 0.4 Hz, $n = 8$), compared to neurons transfected with a scrambled siRNA (28.5 ± 1.7 pA, 4.9 ± 0.6 Hz, $n = 8$). In contrast, the GABA_AR-mediated miniature inhibitory postsynaptic response (mIPSCs) was unchanged by SSH siRNA (Fig. 1C, scrambled siRNA: 26.4 ± 1.2 pA, 3.9 ± 0.4 Hz, $n = 5$; SSH siRNA: 24.6 ± 1.5 pA, 4.1 ± 0.5 Hz, $n = 5$).

Next, we infected cultured cortical slices (DIV 14) with lenti-virus carrying the GFP-tagged SSH shRNA. AMPAR-EPSCs evoked by a series of stimuli were compared in SSH shRNA-infected (GFP⁺) and neighbouring non-infected (GFP⁻) neurons. As shown in Fig. 1D, AMPAR-EPSCs were significantly smaller in neurons infected with SSH shRNA (7 V: 64 ± 12.7 pA; 8 V: 87 ± 16 pA; 9 V: 95 ± 12 pA; $n = 10$), compared to non-infected cells (7 V: 153 ± 8 pA; 8 V: 190 ± 23 pA; 9 V: 205 ± 22 pA; $n = 11$). Moreover, the SSH shRNA-infected neurons showed significantly smaller mEPSC amplitude and frequency (Fig. 1E and F, 10.1 ± 1.2 pA, 1.8 ± 0.2 Hz, $n = 9$) compared to neighbouring non-infected cells (17.0 ± 2.5 pA, 3.4 ± 0.3 Hz, $n = 8$).

We further examined whether acute blockade of the function of endogenous Slingshot could alter AMPAR synaptic responses. As shown in Fig. 2A–C, dialysis with an antibody against Slingshot ($10 \mu\text{g ml}^{-1}$, 30 min) induced a significant reduction of mEPSC amplitude ($41.5 \pm 6.2\%$, $n = 6$) and frequency ($39.8 \pm 4.7\%$, $n = 6$) in cultured cortical neurons, while stable mEPSCs were obtained in neurons dialysed with the heat-inactivated SSH antibody within the same time frame (amplitude: $5.3 \pm 2.1\%$ reduction, $n = 5$; frequency: $5.8 \pm 1.4\%$ reduction, $n = 5$). In cortical slices, the Slingshot antibody significantly reduced the amplitude of evoked AMPAR-EPSCs ($40.3 \pm 4.3\%$, $n = 7$, Fig. 2G), but not NMDAR-EPSCs ($3.2 \pm 5.3\%$, $n = 6$, Fig. 2F). To test the pre- vs. postsynaptic nature of the effect of Slingshot, we measured the paired-pulse ratio (PPR) of AMPAR-EPSCs, a readout that is affected by presynaptic transmitter release. As shown in Fig. 2D and E, PPR was not significantly changed by dialysis with the Slingshot antibody (2.4 ± 0.16 at 5th minute; 2.3 ± 0.16 at 30th minute, $n = 8$), suggesting that presynaptic transmitter release is not altered. Because insertion of AMPARs to the synaptic membrane or removal of synaptic AMPARs could lead to an increase or decrease of the number of functional synapses (Shi *et al.* 1999; Beattie *et al.* 2000), the changes in mEPSC frequency, as well as mEPSC amplitude, with Slingshot inhibition are probably mediated by postsynaptic AMPAR changes.

Given the role of SSH on AMPAR synaptic responses, we further examined whether perturbation of Slingshot function could alter the ability to express synaptic plasticity. Because frontal cortical pyramidal neurons usually do not exhibit electrical stimulation-induced long-term potentiation (LTP; Otani *et al.* 1998; Zhong *et al.* 2008), we measured LTP induced by active Ca^{2+} /calmodulin-dependent protein kinase II (Hayashi *et al.* 2000; Esteban *et al.* 2003). Neurons were dialysed with an EGTA-free internal solution containing purified CaMKII ($0.6 \mu\text{g ml}^{-1}$), calmodulin ($30 \mu\text{g ml}^{-1}$) and CaCl_2 (0.3 mM). As shown in Fig. 2*H* and *I*, dialysis with the active CaMKII caused a sustained potentiation of AMPAR-EPSCs in the presence of the control antibody ($139 \pm 6.2\%$ of baseline, $n = 6$), while this form of LTP was abolished by injecting with the Slingshot antibody ($89.2 \pm 4.3\%$ of baseline, $n = 6$). Taken together, these data suggest that knockdown of SSH expression or blockade

of SSH function selectively reduces AMPAR-mediated synaptic transmission and plasticity.

Slingshot modulates AMPA receptor function via cofilin

The major substrate of Slingshot is cofilin, the actin depolarizing factor (Huang *et al.* 2006). Slingshot dephosphorylation of cofilin at Ser3 allows activating and reactivating processes of cofilin, which enables actin severing and depolymerization (Huang *et al.* 2006). Thus, Slingshot inhibition should keep cofilin in a phosphorylated and inactive state, therefore interfering with the actin dynamics and AMPAR trafficking. To test this, we examined the effect of cofilin inactivation on AMPAR synaptic responses in neurons transfected with SSH siRNA. The phosphorylated (p)-cofilin peptide

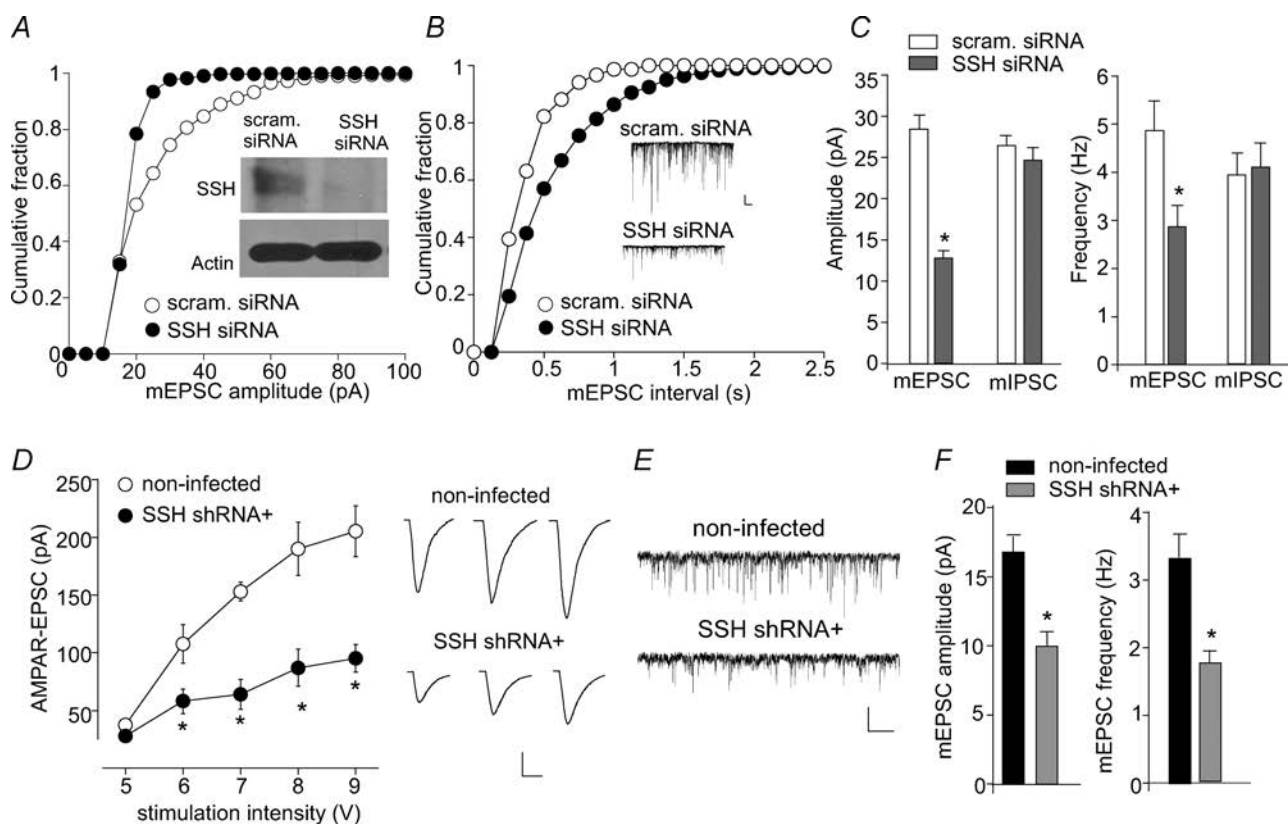


Figure 1. Slingshot knockdown reduces AMPAR-EPSCs in cortical pyramidal neurons

A and *B*, cumulative plots of the distribution of mEPSC amplitude (*A*) or frequency (*B*) in primary cultures transfected with SSH1L siRNA or a scrambled siRNA. Inset (*A*): Western blot analysis showing the level of SSH1L and actin in siRNA-transfected cultures. Inset (*B*): representative mEPSC traces taken from siRNA-transfected neurons. Scale bars: 25 pA, 1 s. *C*, bar graphs summarizing the amplitude (left) and frequency (right) of mEPSC or mIPSC in neurons transfected with different siRNAs. $*P < 0.001$, ANOVA. *D*, summarized input-output curves of AMPAR-EPSCs evoked by a series of stimulation intensities in GFP⁻ (non-infected) vs. GFP⁺ (lenti-SSH shRNA-infected) neurons from cultured cortical slices. Representative EPSC traces are also shown. Scale bars: 50 pA, 20 ms. *E* and *F*, representative mEPSC traces (*E*) and bar graph summary of mEPSCs (mean \pm s.e.m., *F*) in non-infected or SSH shRNA-infected neurons. Scale bars: 20 pA, 1 s. $*P < 0.001$, ANOVA.

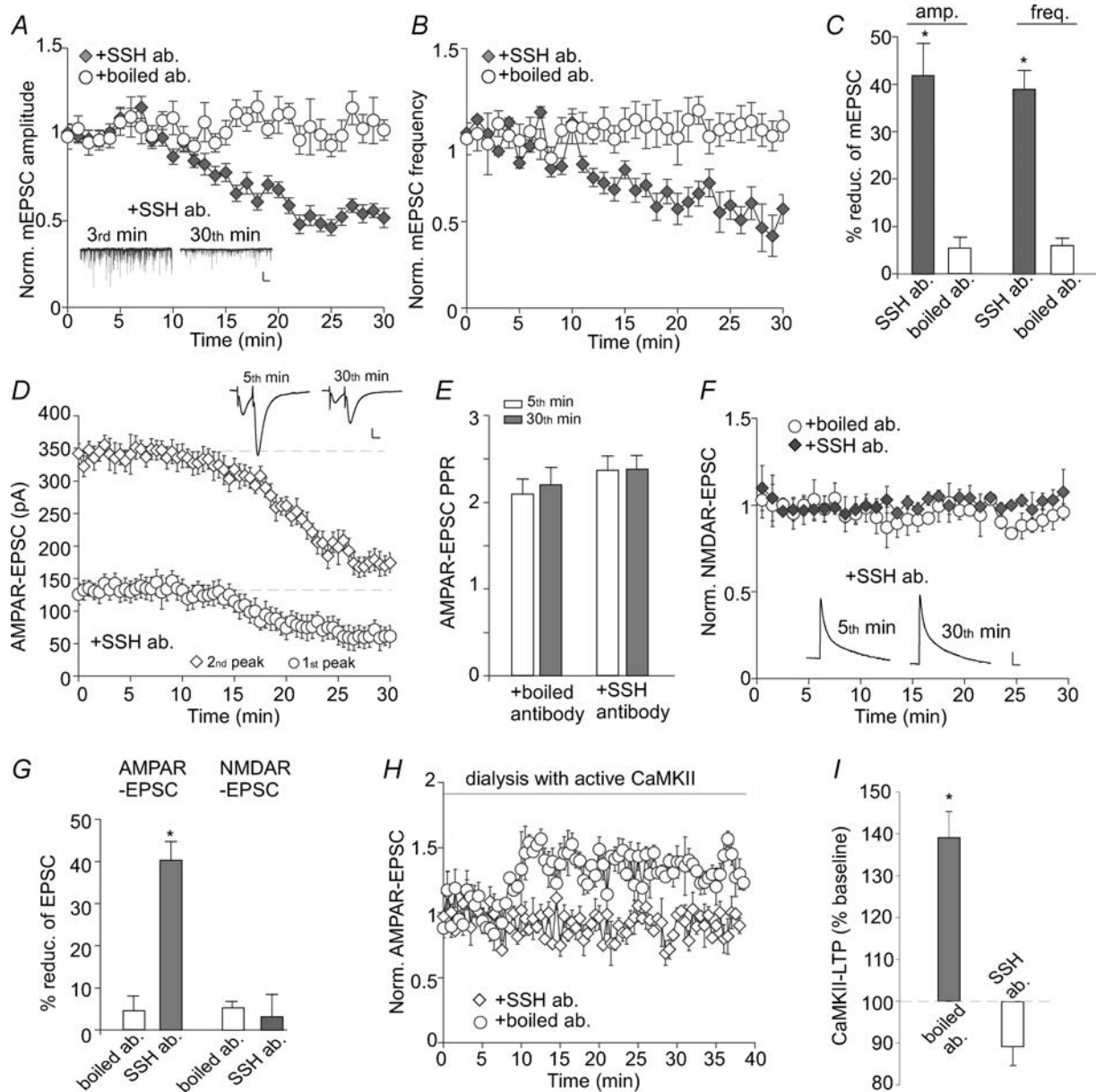


Figure 2. Slingshot inhibition reduces AMPAR-mediated synaptic transmission and blocks the expression of synaptic plasticity

A, plot of normalized mEPSC amplitude (A) and frequency (B) in cultured neurons dialysed with the Slingshot1 antibody ($10 \mu\text{g ml}^{-1}$) vs. heat-inactivated antibody. Inset (A): representative mEPSC traces recorded at 3rd vs. 30th minute in cells injected with anti-Slingshot1. Scale bars: 25 pA, 1 s. C, bar graphs (mean \pm s.e.m.) showing the percentage reduction of mEPSC amplitude or frequency by different antibodies. $*P < 0.001$, ANOVA. D, plot of AMPAR-EPSCs evoked by paired pulses (inter-stimulus interval: 20 ms) in neurons dialysed with the Slingshot1 antibody. Inset: representative eEPSC traces recorded at 5th vs. 30th minute. Scale bars: 50 pA, 10 ms. E, bar graphs (mean \pm s.e.m.) showing the paired-pulse ratio (PPR) of AMPAR-EPSCs in neurons dialysed with different antibodies. F, plot of NMDAR-EPSCs in neurons dialysed with the Slingshot1 antibody vs. heat-inactivated antibody. Inset: representative NMDAR-EPSC traces recorded at 5th vs. 30th minutes. Scale bars: 25 pA, 100 ms. G, bar graphs (mean \pm s.e.m.) showing the percentage reduction of AMPAR-EPSCs or NMDAR-EPSCs in neurons dialysed with different antibodies. $*P < 0.001$, ANOVA. H, plot of normalized AMPAR-EPSCs in neurons dialysed with active CaMKII ($0.6 \mu\text{g ml}^{-1}$) plus the Slingshot1 antibody or heat-inactivated antibody. I, bar graphs (mean \pm s.e.m.) showing the CaMKII-LTP of AMPAR-EPSCs in neurons dialysed with different antibodies. $*P < 0.001$, ANOVA.

(MAS^PGVAVSDGVKVFN) derived from 1–16 residues of cofilin with Ser3 phosphorylation was designed to act as an inhibitor of endogenous cofilin (Aizawa *et al.* 2001; Zhou *et al.* 2004; Yuen & Yan, 2009), because it should bind to endogenous cofilin phosphatases, therefore preventing the dephosphorylation and activation of end-

ogenous cofilin. The non-phosphorylated cofilin peptide serves as a negative control.

As shown in Fig. 3A–C, dialysis with p-cofilin peptide (50 μ M) induced a significant reduction of mEPSC amplitude ($34.8 \pm 2.7\%$, $n = 6$) and frequency ($44.0 \pm 4.9\%$, $n = 6$) in neurons transfected with a

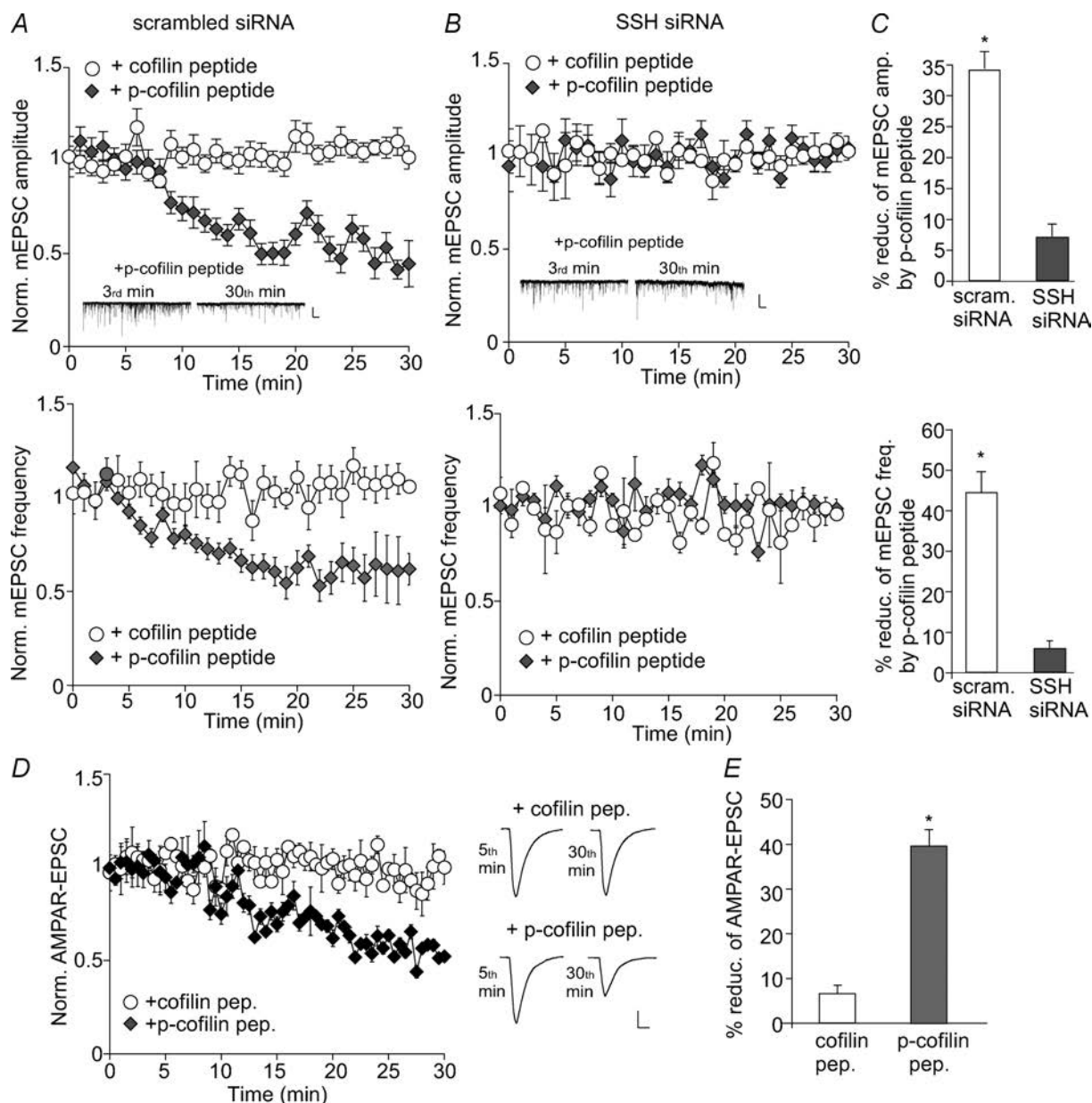


Figure 3. Cofilin, the actin depolymerizing factor, is involved in Slingshot regulation of AMPAR-EPSCs

A and B, plot of normalized mEPSC amplitude (top) and frequency (bottom) showing the effect of dialysis with the p-cofilin peptide vs. the non-phosphorylated cofilin control peptide in cultured cortical neurons transfected with a scrambled siRNA (A) or SSH1L siRNA (B). Inset: representative mEPSC traces recorded at 3rd or 30th minute with p-cofilin peptide dialysis in siRNA-transfected neurons. Scale bars: 25 pA, 1 s. C, bar graphs (mean \pm S.E.M.) illustrating the percentage reduction of mEPSC amplitude (top) and frequency (bottom) by p-cofilin peptide in neurons transfected with different siRNAs. $*P < 0.001$, ANOVA. D, plot of normalized AMPAR-EPSCs in neurons dialysed with cofilin peptide vs. p-cofilin peptide. Inset: representative eEPSC traces recorded at 5th or 30th minute. Scale bars: 25 pA, 10 ms. E, bar graphs (mean \pm S.E.M.) illustrating the percentage reduction of evoked AMPAR-EPSCs by different peptides. $*P < 0.001$, ANOVA.

scrambled siRNA, similar to the effect of SSH inhibition. The cofilin control peptide was ineffective. In neurons transfected with SSH siRNA, p-cofilin failed to significantly reduce mEPSC amplitude ($6.8 \pm 2.0\%$, $n=7$) or frequency ($5.8 \pm 1.9\%$, $n=7$), indicating that the effect of p-cofilin was occluded in neurons with Slingshot knockdown. These data suggest that Slingshot modulates AMPAR synaptic responses through a mechanism involving cofilin.

We further tested whether perturbation of cofilin function could directly impact on AMPARs in cortical slices. As shown in Fig. 3D and E, dialysis with p-cofilin peptide ($50 \mu\text{M}$) significantly reduced the amplitude of evoked AMPAR-EPSCs ($39.6 \pm 3.7\%$, $n=5$), while the inactive cofilin peptide had almost no effect ($6.6 \pm 1.9\%$, $n=5$).

Actin dynamics is involved in Slingshot modulation of AMPA receptor function

The functionality of the actin cytoskeleton depends on a dynamic equilibrium between filamentous and monomeric actin. Cofilin protein is essential for the high rates of actin filament turnover through regulation of actin polymerization/depolymerization cycles (dos Remedios *et al.* 2003). We speculate that perturbation of actin dynamics by cofilin may underlie Slingshot regulation of AMPAR synaptic responses. To test this, we measured the effect of actin stabilizer, a condition mimicking cofilin inhibition, on mEPSCs in cultured cortical neurons transfected with SSH siRNA. As shown in Fig. 4A–C, dialysis of the actin stabilizer phalloidin ($5 \mu\text{M}$) significantly reduced mEPSC amplitude ($45.4 \pm 2.4\%$, $n=6$) and frequency ($46.0 \pm 4.4\%$, $n=6$) in scrambled siRNA-transfected neurons, similar to the effect of SSH suppression or cofilin inhibition. However, the effect of phalloidin on mEPSCs was lost in neurons transfected with SSH siRNA (amplitude (amp.): $4.8 \pm 1.4\%$; frequency (freq.): $8.2 \pm 4.3\%$, $n=7$). Another actin stabilizer, jasplakinolide ($10 \mu\text{M}$), also significantly reduced mEPSCs in scrambled siRNA-transfected neurons (amp.: $40.2 \pm 2.6\%$; freq.: $39.9 \pm 5.1\%$, $n=5$), but not in SSH siRNA-transfected neurons (amp.: $5.1 \pm 2.5\%$; freq.: $5.3 \pm 4.7\%$, $n=7$). These data suggest that Slingshot modulates AMPAR synaptic responses through a mechanism involving actin dynamics.

Next, we performed immunocytochemical experiments in neuronal cultures to directly measure the impact of Slingshot on actin dynamics. As shown in Fig. 4D and E, knockdown of SSH caused a significant reduction of F-actin cluster density (no. clusters ($50 \mu\text{m dendrite}^{-1}$) (scrambled siRNA: 20.4 ± 2.9 , $n=8$; SSH siRNA: 9.8 ± 1.4 , $n=8$; $P < 0.001$, ANOVA). It suggests that SSH is important for maintaining the dynamic

equilibrium between filamentous and monomeric actin.

Slingshot inhibition reduces surface AMPAR clusters through an actin-dependent mechanism

Next, we examined whether the effect of Slingshot/cofilin/actin on AMPAR synaptic responses was due to the changes in AMPAR membrane trafficking. Surface AMPAR expression was measured in cultured cortical neurons transfected with SSH siRNA. As shown in Fig. 5A–C, surface GluR1 clusters were significantly reduced in SSH siRNA-transfected neurons (cluster density: 15.2 ± 1.6 ($50 \mu\text{m dendrite}^{-1}$); cluster size: $0.21 \pm 0.03 \mu\text{m}^2$; intensity: 59.2 ± 3.3 , $n=8$), compared to scrambled siRNA-transfected neurons (cluster density: 31.5 ± 2.0 ($50 \mu\text{m dendrite}^{-1}$); cluster size: $0.31 \pm 0.03 \mu\text{m}^2$; intensity: 96.0 ± 5.2 , $n=9$). Application of the membrane-permeable (myristoylated) phalloidin ($5 \mu\text{M}$, 30 min) caused a significant reduction of surface GluR1 clusters (cluster density: 15.1 ± 2.1 ($50 \mu\text{m dendrite}^{-1}$); cluster size: $0.2 \pm 0.03 \mu\text{m}^2$; intensity: 58.0 ± 3 , $n=10$) in scrambled siRNA-transfected neurons. However, phalloidin failed to further reduce surface GluR1 clusters in SSH siRNA-transfected neurons (cluster density: 15.0 ± 1.9 ($50 \mu\text{m dendrite}^{-1}$); cluster size: $0.19 \pm 0.04 \mu\text{m}^2$; intensity: 56.9 ± 3.2 , $n=10$).

Finally, we examined whether the trafficking of GluR2/3 subunits are also regulated by Slingshot. Synaptic GluR2/3 clusters were measured by detecting GluR2/3 co-localized with the synaptic marker synaptophysin. As shown in Fig. 5D and E, SSH siRNA-transfected neurons showed a significant reduction of synaptic GluR2/3 cluster density (no. clusters ($50 \mu\text{m dendrite}^{-1}$) (scrambled siRNA: 13.7 ± 1.6 , $n=9$; SSH siRNA: 7.6 ± 0.7 , $n=9$; $P < 0.01$, ANOVA). The synaptophysin clusters were not significantly altered by Slingshot knockdown (scrambled siRNA: 32.1 ± 2.7 , $n=9$; SSH siRNA: 27.7 ± 1.4 , $n=9$; $P > 0.05$, ANOVA), suggesting the lack of changes in synapses. Taken together, these data suggest that Slingshot modulates AMPAR trafficking through an actin-dependent mechanism.

Discussion

The Slingshot family of protein phosphatases is abundantly expressed in the brain, and specifically dephosphorylates cofilin *in vitro* and *in vivo* (Endo *et al.* 2003; Ohta *et al.* 2003). While Slingshot has been implicated in cell division, growth cone motility and neurite extension through cofilin regulation (Huang *et al.* 2006), the role of Slingshot in regulating synaptic function is largely unknown. In this study,

we found that knockdown of Slingshot expression or blockade of Slingshot function significantly impaired AMPAR-mediated synaptic responses, consequently diminishing the ability to express synaptic plasticity.

Consistent with the central role of AMPAR dynamics in synaptic plasticity (Hayashi *et al.* 2000; Malinow & Malenka, 2002; Esteban *et al.* 2003), AMPAR GluR1 surface expression and GluR2/3 synaptic expression were

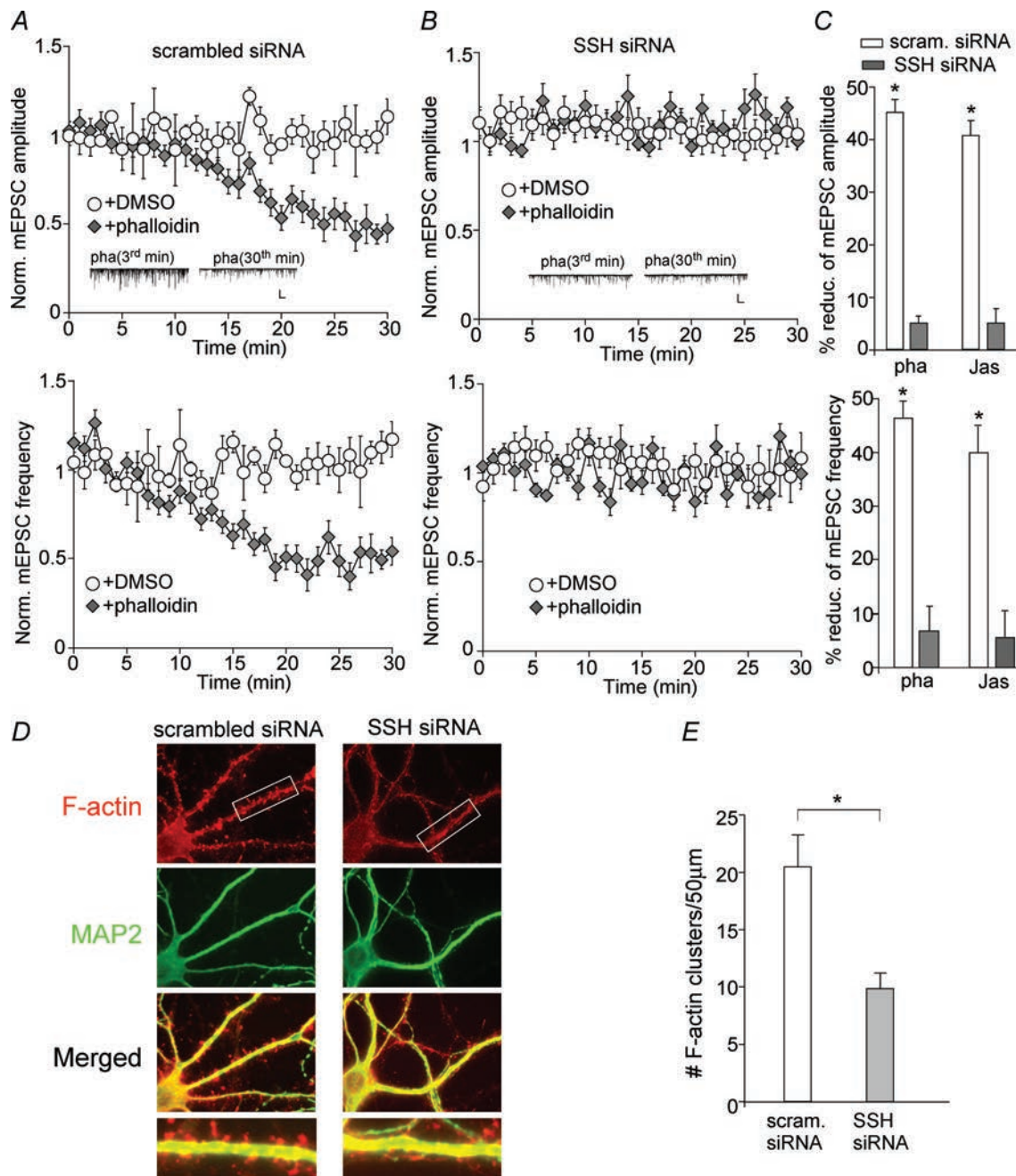


Figure 4. Slingshot regulates AMPAR-EPSCs by interfering with actin dynamics

A and **B**, plot of normalized mEPSC amplitude (top) and frequency (bottom) showing the effect of dialysis with the actin stabilizer phalloidin (10 μ M) or DMSO vehicle (0.1%) in cultured cortical neurons transfected with a scrambled siRNA (**A**) or SSH1L siRNA (**B**). Inset: representative mEPSC traces at 3rd or 30th minute with phalloidin dialysis in siRNA-transfected neurons. Scale bars: 25 pA, 1 s. **C**, bar graphs (mean \pm s.e.m.) showing the percentage reduction of mEPSC amplitude (top) and frequency (bottom) by actin stabilizer phalloidin or jasplakinolide in neurons transfected with different siRNAs. $*P < 0.001$, ANOVA. **D**, immunocytochemical images of F-actin (red) and MAP2 (green) in cultured cortical neurons transfected with a scrambled siRNA or SSH1L siRNA. **E**, quantitative analysis of F-actin cluster density on dendrites of neurons transfected with different siRNAs. $*P < 0.001$, ANOVA.

also reduced by Slingshot knockdown, which could be due to the diminished membrane trafficking and synaptic delivery of AMPARs, or reduced retention of AMPARs at the synapse.

Cofilin, the major F-actin-severing protein, has been implicated in the regulation of spine cytoskeleton and morphology (Carlisle *et al.* 2008). The Ser3 site of cofilin provides a phosphoregulatory switch for actin

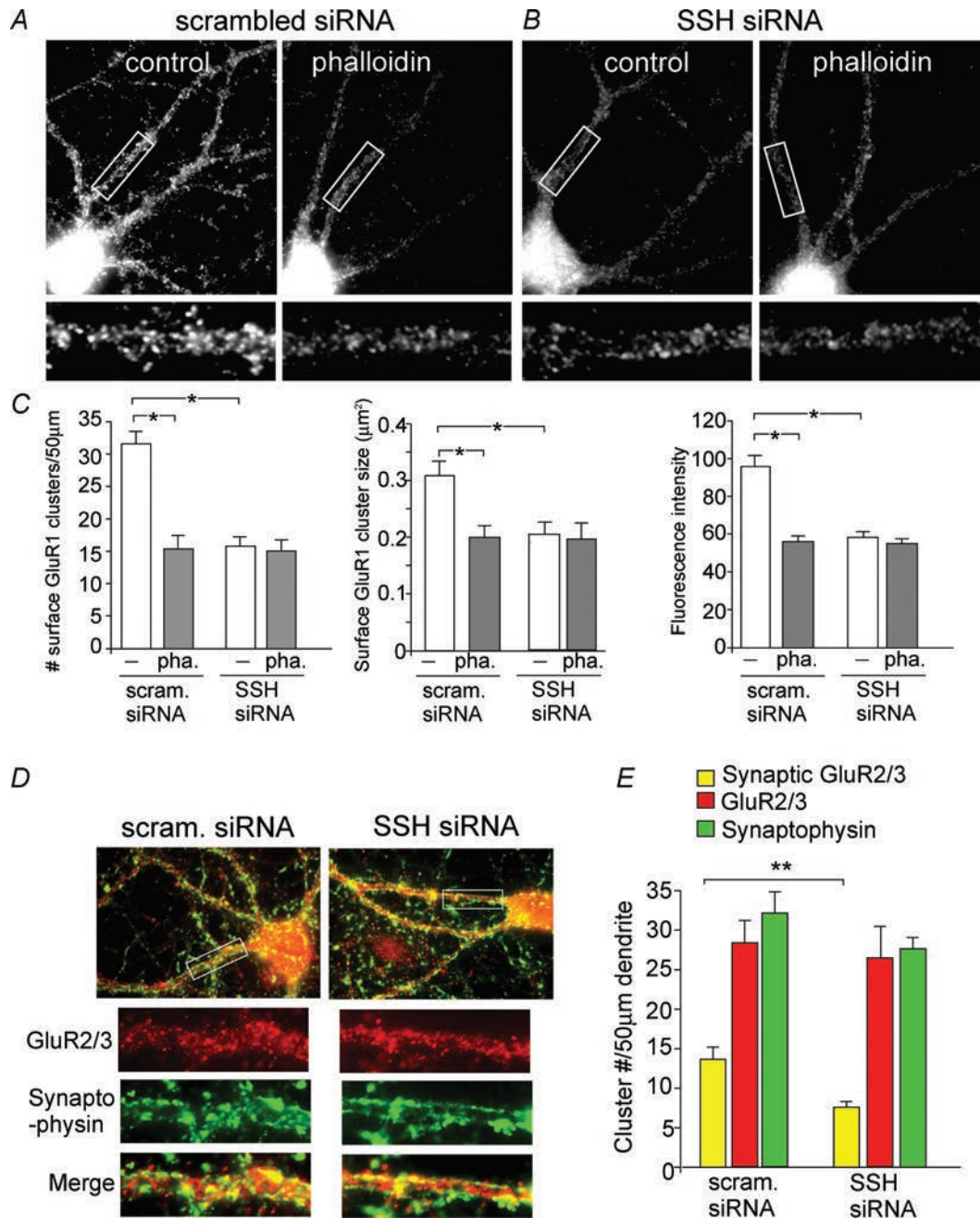


Figure 5. Slingshot inhibition perturbs AMPAR trafficking via an actin-dependent mechanism

A and *B*, immunocytochemical images showing the effect of myristoylated phalloidin (10 µM, 30 min) on surface GluR1 clusters in cultured cortical neurons transfected with a scrambled siRNA (*A*) or SSH1L siRNA (*B*). *C*, quantitative analysis of surface GluR1 clusters (density, intensity, and size) on dendrites in control vs. phalloidin-treated neurons transfected with different siRNAs. **P* < 0.001, ANOVA. *D* and *E*, immunocytochemical images (*D*) and quantitative analysis (*E*) of synaptic GluR2/3 (synaptophysin co-localized, yellow puncta), total GluR2/3 clusters (red puncta) and synaptophysin clusters (green puncta) along dendrites in cultured cortical neurons transfected with a scrambled siRNA or SSH1L siRNA. Enlarged versions of the boxed regions of dendrites are also shown. ***P* < 0.01, ANOVA.

polymerization and depolymerization (Morgan *et al.* 1993; Huang *et al.* 2006). Inhibiting endogenous cofilin by the Ser3-p-cofilin peptide blocks the actin-dependent NMDAR-induced long-term depression (LTD) (Morishita *et al.* 2005) and spine shrinkage associated with AMPAR-LTD (Zhou *et al.* 2004). In this study, we found that application of the cofilin inhibitory peptide produced a reducing effect on mEPSCs, which was occluded by Slingshot suppression. It suggests that Slingshot modulation of AMPAR-mediated synaptic transmission is dependent on cofilin activity.

Actin cytoskeleton undergoes rapid transitions between polymerization and depolymerization processes. Mounting evidence suggests the importance of actin in receptor anchoring (Shen *et al.* 2000; Rocca *et al.* 2008), spine reorganization (Okamoto *et al.* 2004) and AMPAR transport (Lise *et al.* 2006; Correia *et al.* 2008). Actin depolymerization induces AMPAR internalization (Zhou *et al.* 2001) and impairs synaptic transmission and plasticity (Fukazawa *et al.* 2003; Yuen & Yan, 2009), but less is known regarding the consequences of actin polymerization. Downregulation of Slingshot by siRNA should prevent cofilin activation, thereby switching actin to the polymerized state. In this study, we found that application of actin stabilizers reduced mEPSCs and surface GluR1 expression, consistent with a previous study showing that phalloidin reduces AMPA receptor-mediated synaptic transmission in hippocampal slices (Kim & Lisman, 2001). Thus, changing the balance of filamentous and monomeric actin in either direction reduces the number of synaptic AMPARs. Our data also indicated that the inhibitory effect of actin stabilizer on AMPARs was occluded by Slingshot suppression, suggesting that Slingshot regulates AMPAR trafficking and function by altering the actin dynamics.

In summary, we have revealed a new mechanism by which AMPAR trafficking and synaptic plasticity can be controlled, i.e. through the phosphatase Slingshot, a key modulator of cofilin activity and actin dynamics.

References

- Agnew BJ, Minamide LS & Bamberg JR (1995). Reactivation of phosphorylated actin depolymerizing factor and identification of the regulatory site. *J Biol Chem* **270**, 17582–17587.
- Aizawa H, Wakatsuki S, Ishii A, Moriyama K, Sasaki Y, Ohashi K, Sekine-Aizawa Y, Sehara-Fujisawa A, Mizuno K, Goshima Y & Yahara I (2001). Phosphorylation of cofilin by LIM-kinase is necessary for semaphorin 3A-induced growth cone collapse. *Nat Neurosci* **4**, 367–373.
- Beattie EC, Carroll RC, Yu X, Morishita W, Yasuda H, von Zastrow M & Malenka RC (2000). Regulation of AMPA receptor endocytosis by a signalling mechanism shared with LTD. *Nat Neurosci* **3**, 1291–1300.
- Carlisle HJ, Manzerra P, Marcora E & Kennedy MB (2008). SynGAP regulates steady-state and activity-dependent phosphorylation of cofilin. *J Neurosci* **28**, 13673–13683.
- Correia SS, Bassani S, Brown TC, Lise MF, Backos DS, El-Husseini A, Passafaro M & Esteban JA (2008). Motor protein-dependent transport of AMPA receptors into spines during long-term potentiation. *Nat Neurosci* **11**, 457–466.
- Derkach VA, Oh MC, Guire ES & Soderling TR (2007). Regulatory mechanisms of AMPA receptors in synaptic plasticity. *Nat Rev Neurosci* **8**, 101–113.
- dos Remedios CG, Chhabra D, Kekic M, Dedova IV, Tsubakihara M, Berry DA, Nosworthy NJ (2003). Actin binding proteins: regulation of cytoskeletal microfilaments. *Physiol Rev* **83**, 433–473.
- Endo M, Ohashi K, Sasaki Y, Goshima Y, Niwa R, Uemura T & Mizuno K (2003). Control of growth cone motility and morphology by LIM kinase and Slingshot via phosphorylation and dephosphorylation of cofilin. *J Neurosci* **23**, 2527–2537.
- Esteban JA, Shi SH, Wilson C, Nuriya M, Haganir RL & Malinow R (2003). PKA phosphorylation of AMPA receptor subunits controls synaptic trafficking underlying plasticity. *Nat Neurosci* **6**, 136–143.
- Fukazawa Y, Saitoh Y, Ozawa F, Ohta Y, Mizuno K & Inokuchi K (2003). Hippocampal LTP is accompanied by enhanced F-actin content within the dendritic spine that is essential for late LTP maintenance in vivo. *Neuron* **38**, 447–460.
- Gu Z, Jiang Q, Yuen EY & Yan Z (2006). Activation of dopamine D4 receptors induces synaptic translocation of Ca²⁺/calmodulin-dependent protein kinase II in cultured prefrontal cortical neurons. *Mol Pharmacol* **69**, 813–822.
- Hayashi Y, Shi SH, Esteban JA, Piccini A, Poncer JC & Malinow R (2000). Driving AMPA receptors into synapses by LTP and CaMKII: requirement for GluR1 and PDZ domain interaction. *Science* **287**, 2262–2267.
- Huang TY, DerMardirossian C & Bokoch GM (2006). Cofilin phosphatases and regulation of actin dynamics. *Curr Opin Cell Biol* **18**, 26–31.
- Kim CH & Lisman JE (2001). A labile component of AMPA receptor-mediated synaptic transmission is dependent on microtubule motors, actin, and N-ethylmaleimide-sensitive factor. *J Neurosci* **21**, 4188–4194.
- Lin B, Kramar EA, Bi X, Brucher FA, Gall CM & Lynch G (2005). Theta stimulation polymerizes actin in dendritic spines of hippocampus. *J Neurosci* **25**, 2062–2069.
- Lise MF, Wong TP, Trinh A, Hines RM, Liu L, Kang R, Hines DJ, Lu J, Goldenring JR, Wang YT & El-Husseini A (2006). Involvement of myosin Vb in glutamate receptor trafficking. *J Biol Chem* **281**, 3669–3678.
- Malinow R & Malenka RC (2002). AMPA receptor trafficking and synaptic plasticity. *Annu Rev Neurosci* **25**, 103–126.
- Meng Y, Zhang Y, Tregoubov V, Janus C, Cruz L, Jackson M, Lu WY, MacDonald JF, Wang JY, Falls DL & Jia Z (2002). Abnormal spine morphology and enhanced LTP in LIMK-1 knockout mice. *Neuron* **35**, 121–133.
- Morgan TE, Lockerbie RO, Minamide LS, Browning MD & Bamberg JR (1993). Isolation and characterization of a regulated form of actin depolymerizing factor. *J Cell Biol* **122**, 623–633.

- Morishita W, Marie H & Malenka RC (2005). Distinct triggering and expression mechanisms underlie LTD of AMPA and NMDA synaptic responses. *Nat Neurosci* **8**, 1043–1050.
- Niwa R, Nagata-Ohashi K, Takeichi M, Mizuno K & Uemura T (2002). Control of actin reorganization by Slingshot, a family of phosphatases that dephosphorylate ADF/cofilin. *Cell* **108**, 233–246.
- Ohta Y, Kousaka K, Nagata-Ohashi K, Ohashi K, Muramoto A, Shima Y, Niwa R, Uemura T & Mizuno K (2003). Differential activities, subcellular distribution and tissue expression patterns of three members of Slingshot family phosphatases that dephosphorylate cofilin. *Genes Cells* **8**, 811–824.
- Okamoto K, Nagai T, Miyawaki A & Hayashi Y (2004). Rapid and persistent modulation of actin dynamics regulates postsynaptic reorganization underlying bidirectional plasticity. *Nat Neurosci* **7**, 1104–1112.
- Otani S, Blond O, Desce JM & Crepel F (1998). Dopamine facilitates long-term depression of glutamatergic transmission in rat prefrontal cortex. *Neuroscience* **85**, 669–676.
- Rocca DL, Martin S, Jenkins EL & Hanley JG (2008). Inhibition of Arp2/3-mediated actin polymerization by PICK1 regulates neuronal morphology and AMPA receptor endocytosis. *Nat Cell Biol* **10**, 259–271.
- Shen L, Liang F, Walensky LD & Huganir RL (2000). Regulation of AMPA receptor GluR1 subunit surface expression by a 4.1N-linked actin cytoskeletal association. *J Neurosci* **20**, 7932–7940.
- Shi SH, Hayashi Y, Petralia RS, Zaman SH, Wenthold RJ, Svoboda K & Malinow R (1999). Rapid spine delivery and redistribution of AMPA receptors after synaptic NMDA receptor activation. *Science* **284**, 1811–1816.
- Stoppini L, Buchs PA & Muller D (1991). A simple method for organotypic cultures of nervous tissue. *J Neurosci Methods* **37**, 173–182.
- Wang Z, Edwards JG, Riley N, Provance DW Jr, Karcher R, Li XD, Davison IG, Ikebe M, Mercer JA, Kauer JA & Ehlers MD (2008). Myosin Vb mobilizes recycling endosomes and AMPA receptors for postsynaptic plasticity. *Cell* **135**, 535–548.
- Wang Y, Shibasaki F & Mizuno K (2005). Calcium signal-induced cofilin dephosphorylation is mediated by Slingshot via calcineurin. *J Biol Chem* **280**, 12683–12689.
- Yuen EY, Gu Z & Yan Z (2007). Calpain regulation of AMPA receptor channels in cortical pyramidal neurons. *J Physiol* **580**, 241–254.
- Yuen EY, Jiang Q, Chen P, Gu Z, Feng J & Yan Z (2005). Serotonin 5-HT_{1A} receptors regulate NMDA receptor channels through a microtubule-dependent mechanism. *J Neurosci* **25**, 5488–5501.
- Yuen EY & Yan Z (2009). Dopamine D₄ receptors regulate AMPA receptor trafficking and glutamatergic transmission in GABAergic interneurons of prefrontal cortex. *J Neurosci* **29**, 550–562.
- Zhong P, Liu W, Gu Z & Yan Z (2008). Serotonin facilitates long-term depression induction in prefrontal cortex via p38 MAPK/Rab5-mediated enhancement of AMPA receptor internalization. *J Physiol* **586**, 4465–4479.
- Zhou Q, Homma KJ & Poo MM (2004). Shrinkage of dendritic spines associated with long-term depression of hippocampal synapses. *Neuron* **44**, 749–757.
- Zhou Q, Xiao M & Nicoll RA (2001). Contribution of cytoskeleton to the internalization of AMPA receptors. *Proc Natl Acad Sci U S A* **98**, 1261–1266.

Author contributions

E.Y.Y. performed experiments and analysed data. W.L. performed experiments. T.K. and H.v.P. generated key reagents. Z.Y. designed the experiments and wrote the paper. The experiments were done in SUNY-Buffalo. All authors approved the final version of the manuscript.

Acknowledgements

This work was supported by grants from the National Institutes of Health to Z.Y. We would like to thank Xiaoqing Chen for her technical support.